ORIGINAL ARTICLE

Variation of rill cross-sections with gravel and aggregating soil in the Dry-Hot Valley (SW China)

Nana Wang[1,3] · Lin Ding[1,4] · Gangcai Liu[2] · Qingchun Deng[1,3] · Hui Liu[1,3] · Jie Wang[1,3] · Wei Lv[1,3] · Jun Luo[1,3] · Ziyin Du[1,3] · Bin Zhang[1,3]

Abstract

Cross-sectional morphology is an effective approach for calculating rill volume and revealing the mechanism for rill development. In this study, the law governing the temporal–spatial variation in rill cross-section (RCS) under interbedded clay and gravel conditions was investigated by a scouring experiment. A high-flow scouring experiment was conducted in a field plot under heterogeneous soil conditions in the Yuanmou Dry-Hot Valley using 3D laser scanning and ArcGIS techniques. Morphological index system including the size and derived proportional parameters was established to accurately reveal the dynamic process of the rill erosion–sediment sections based on temporal–spatial scale. The study indicated that the RCS size under gravel and soil aggregates showed an irregular variation over different periods, and the variation of RCS morphology tends to be nonlinear. The area of rill cross-section at the middle of the rill was much larger than that of the rill head and the rill mouth, and the fluctuations in RCS along the rill depended heavily on the soil texture heterogeneity. In addition, there were extreme variations in rill erosion direction for different rill parts, i.e., rill head, body, and mouth, and the highly significant asymmetry in RCS distributed along the rill under increasing scouring duration in the Yuanmou Dry-Hot valley. Temporal variations in RCS morphology were opposite to spatial variations by comparing the same morphology parameter. Nonlinear fluctuation trends and asymmetric shapes were observed in the variation of RCS on slopes with soils and gravels.

Keywords Rill cross-section · Temporal–spatial variation · Scouring experiment · Gravel and soil aggregates

Introduction

Rills are a type of small-groove topography produced by slope runoff under differential erosion conditions (He et al. 2016), which function as both sediment sources and sediment transport vehicles on slopes (Ma et al. 2017a). With rill development and variation, subsequent rill erosion has gradually turned into a major form of soil erosion on slopes (Yan et al. 2010). It is a process in which the overland flow scours the surface and transports sediments after converging into a stream along the free slope and forms small channels at places where soil erosion resistance is less than the runoff scouring capability. Rill erosion is a transitional stage of slope erosion, toward channel erosion (Yuan and Chang 2008). With the aggravation of erosion process, the slope topography of river basin will change obviously (Yermolaev et al. 2018).

Rill morphology, including planar, cross-sectional, and longitudinal profiles, represents a link between past, present, and future channel erosion activities (Gao 2011) and provides the basis for evaluating erosion amount and evolution stage (Bennett et al. 2015). Rill cross-section (RCS) morphology is the result of scouring between the rill flow and bank soil, which can be applied to analyze the development of rill and the change of energy of rill flow (Hao et al. 2017). During rill expansion, the cross-sectional

✉ Bin Zhang
  envgeo@163.com

1. School of Land and Resources, China West Normal University, Nanchong 637009, People's Republic of China

2. Institute of Mountain Hazards and Environment, Chinese Academy of Sciences, Chengdu 610045, People's Republic of China

3. Sichuan Provincial Engineering Laboratory of Monitoring and Control for Soil Erosion of Dry Valley, China West Normal University, Nanchong 637009, People's Republic of China

4. Faculty of Geographical Science, Beijing Normal University, Beijing 100875, People's Republic of China

morphology tends to be irregular due to the erosional resistance of bottom soil and different stages of rill development (Govers 1992; Mancilla et al. 2005), although the cross-sections in the lower part of the channel are generally larger than those in the upper part (Shen et al. 2015b). Overall, the RCS has a rectangular or trapezoidal shape (Yang et al. 2006; Zhang et al. 2007), but its most common forms are U-shape and V-shape (Zhang et al. 2014). Precise RCS data are crucial for calculating erosion volume and rate (Capra et al. 2010; Frankl et al. 2013), and also helpful for revealing the erosion process (Heede 1970; Stefano et al. 2013). RCS morphological parameters primarily include rill width (W), depth (D), cross-section erosional area (A) (Frankl et al. 2013; Gabet and Bookter 2008), and other complex quantitative parameters. W is an effective parameter for connecting the RCS to the planar shape, and is more variable than D (Bewket and Sterk 2003). For cultivated soil, the value of W is approximately 15–18 cm, which cuts down to the bottom of the plough layer; for non-cultivated soil, the D value is around 1.5–2 cm, while the value of W varies between 24 and 34 cm, typically 25 cm, and the deep-cutting depth is 4–5 cm (Eltner et al. 2015; Loch and Donnollan 1989). Because the value of W varies widely, D is used for rill size classification, with the following groups: small (15 cm), medium (16–30 cm), large (31–45 cm), and extra-large (46 cm) (Bewket and Sterk 2003). For rills with bed slopes above 3%, the deep-cutting depth increases with the headward erosion of the rill, while larger bed slopes will result in deeper scouring pits (Bennett 1999; Stefano et al. 2018). These parameters often differ significantly at across multiple locations of rill and do not always follow a normal distribution (Green et al. 2007; Zhang et al. 2018). Thus it can be seen that the evolution of RCS morphology is not a one-dimensional development process, but a multi-dimensional change process (Zhang et al. 2018). In addition, relevant proportional parameters can be used to describe RCS morphology, such as the index using width/depth ratio ($R_{w/d}$) and the ratio of the RCS area to the area of an equally wide and deep rectangle (Ran et al. 2018; Zhang and Tang 2000). The morphology can also be described by the cross-sectional coefficient that is calculated as a function of the wetted perimeter and cross-sectional area (Moore and Burch 1986). The RCS morphology shows an obvious spatial–temporal variability under different soil conditions. Generally, the RCS morphology often presents a highly significant linear change under a homogeneous soil matrix (Moore and Burch 1986; Shen et al. 2015a); the value of W varies widely along the rill and $R_{w/d}$ decreases gradually with increasing slope (Berger et al. 2010); the cross-sectional shape transforms from a wide-shallow to narrow-deep with increasing slope (Wang et al. 2015) or is in a small concave-groove shape in early stage of rill development, after which the entire rill bank is completely integrated into the slope and the cross-section

shows an extremely open V-shape (Liu et al. 1988). For heavy and moderate silt loam slopes, the growth of both the values for D and W decelerates with the slope length, and the cross-sections have a shape ratio ranging between 0.40 and 0.85, transitioning from the narrow-deep to the wide-shallow shape (Li 2015). Based on the feedback relationship between rill morphology and sediment yield, the cross-sectional shape at the initial stage of rill development is a V-shape, which changes gradually to a U-shape along with headward and lateral erosion development (Mahmoodabadi et al. 2014). In general, the RCS continues to deepen as development progresses, RCS morphology formed under different rainfall intensity and slope vary; W values change widely along the course, and $R_{w/d}$ values decrease gradually with increasing slope (Berger et al. 2010; He et al. 2013; Shen et al. 2015b). Under natural rainfall conditions, RCS morphological development has general stages: V-shape, U shape, and small upper opening-large bottom opening (Wang et al. 1988; Li 2015). Recent studies of rill erosion under the same soil texture, conducted in laboratories or fields under simulated rainfall or natural conditions (Bruno et al. 2010; Bryan et al. 1989; Rejman and Brodowski 2010), have often focused on the critical conditions for variations in rills cross-section and the formation of rill networks (Bruno et al. 2010; Brunton and Bryan 2015; Slattery and Bryan 1992), the development of rill morphology, and evaluating hydraulic variables (Gilley et al. 1990; Giménez et al. 2010; Meyer et al. 1984) to propose mathematical models that estimate soil loss resulting from rill erosion (Cao et al. 2014; Foster 1982; Nearing et al. 1989; Stefano et al. 2016).

Although more attention is given to rill cross-section morphology and significant progress has been made, some limitations remain. First, most research on rill erosion pattern variations have focused on the overall morphological characteristics after the completion of rill development. Second, studies evaluating rill development under a heterogeneous soil matrix or variation in RCS morphology are still lacking. Third, one-dimensional morphological parameters, such as rill length and width, can briefly reflect the characteristics of a cross-section, but are unable to characterize detailed variations in morphology. Finally, the dynamic process of rill erosion formation or local differences in morphological development remains unclear. To address these limitations, a field scouring experiment to study rill erosion with detailed measurements was conducted under heterogeneous soil conditions. Present study aims to reveal the temporal–spatial variation law governing RCS morphology by establishing a multiple parameter system in the Yuanmou Dry-Hot Valley with gravel and soil aggregates. This study will aid in understanding rill evolutionary mechanisms under different environmental conditions and will contribute to scientific guidance for the prevention and control of rill erosion on sloping lands.

Materials and methods

Study area

The Yuanmou Dry-Hot Valley is located in the northern part of the Middle Yunnan Plateau, China, at an elevation of 980–1400 m and between 101°35′–102°06′E and 25°23′–26°06′N. The Longchuanjiang River flows through the Yuanmou Basin from south to north. There are distinct wet and dry seasons, with an average annual temperature of 21.9 °C, which results in intense surface evaporation. Vegetation consists mainly of shrub grassland and disconnected forest. The zonal soil type in the valley is a typical dry-red aggregated soil with gravel that has experienced serious water and soil loss due to environmental conditions and human activity. Under these conditions, the Yuanmou Dry-Hot Valley has become a typical ecologically fragile and soil eroded region.

The study field plot is located in the Julin Experimental Base of the Huangguayuan Town, Yuanmou County (Fig. 1). The sloping fields in the area have been extensively cultivated to cope with the pressure of rapid population growth. However, when soil on sloping land is farmed improperly, it begins to move under the influence of heavy rainfall.

RCS morphology parameters

The size and derived proportional parameters can be used to accurately depict RCS morphology (Fig. 2). The size parameters are: rill depth (D), width (W), and cross-sectional erosional area (A). D and W reflect the horizontal and vertical ductility as well as the degree of RCS development. D includes the depth of the left side (D_l) and right side (D_r), which reflects the degrees of deep-cutting erosion on the left and right sides of the rill, respectively. W includes the left width (W_l), right width (W_r), and top width (W_t). W_l and W_r of the rill reflect the degrees of leftward or rightward erosion, while the W_t reflects the degree of lateral erosion. A describes the size of the RCS, thus revealing the degree and intensity of rill erosion. The derived proportional parameters include the rill width/depth ratio ($R_{w/d}$), asymmetry ratio of width (A_w), and two shape indices, the shape factor (S_f) and shape ratio (η).

Rill width/depth ratio ($R_{w/d}$)

$R_{w/d}$ refers to the ratio of the rill top width to its maximum depth (Ma et al. 2017b), i.e.,

$$R_{w/d} = W_t \big/ \max(D_l, D_r). \tag{1}$$

It can be used to describe the relationship between lateral erosion and incision. A greater $R_{w/d}$ indicates a more severe lateral rill erosion, milder incision, and shallow U-shaped RCS. A smaller value of $R_{w/d}$ signifies milder lateral rill erosion, more severe incision, and deep V-shaped RCS.

Asymmetry ratio of width (A_w)

The A_w is the ratio of the rill left width to its right width, i.e.,

$$A_w = W_l \big/ W_r. \tag{2}$$

The asymmetry ratio of width is an important parameter to describe the asymmetry of the distance between the left and right erosions of the rill, thereby reflecting the degree of difference in lateral erosion. When $A_w > 1$, the left width of the RCS is greater than the right width, and left erosion prevails; when $A_w = 1$, the degree of the left erosion is the same as that of the right erosion; and when $A_w < 1$, the left width of the RCS is less than the right width, and right erosion prevails.

Shape factor (S_f)

S_f is denoted by:

$$S_f = \max(D_l, D_r) \big/ (A / W_t). \tag{3}$$

When $S_f = 1.0$, the RCS is rectangular; when $S_f = 1.5$, the RCS is parabolic; and when $S_f = 2.0$, the RCS is triangular (Heede 1970; Rustomji 2006).

Shape ratio (η)

η is the ratio of the RCS erosional area (A) to the rectangular area (Ra), with the same top width and maximum rill depth, which is generally expressed as:

$$\eta = A / Ra. \tag{4}$$

η values range between 0 and 1. A smaller η value indicates that the RCS is most similar to a narrow-deep shape; an η value close to 0.5 indicates an RCS shape close to an inverted triangle; and a greater η value indicates that the RCS is most similar to a wide-shallow shape (Zhang and Tang 2000).

Experimental procedures

Experimental design

A scouring experimental plot was configured at the Julin Experimental Base in the Yuanmou Dry-Hot Valley region. The plot was 20 m long, 5 m wide and 1 m high, with a westward aspect. It descended from east to west,

Fig. 1 Study site in the Julin experimental base of the Huangguayuan Town, Yuanmou County
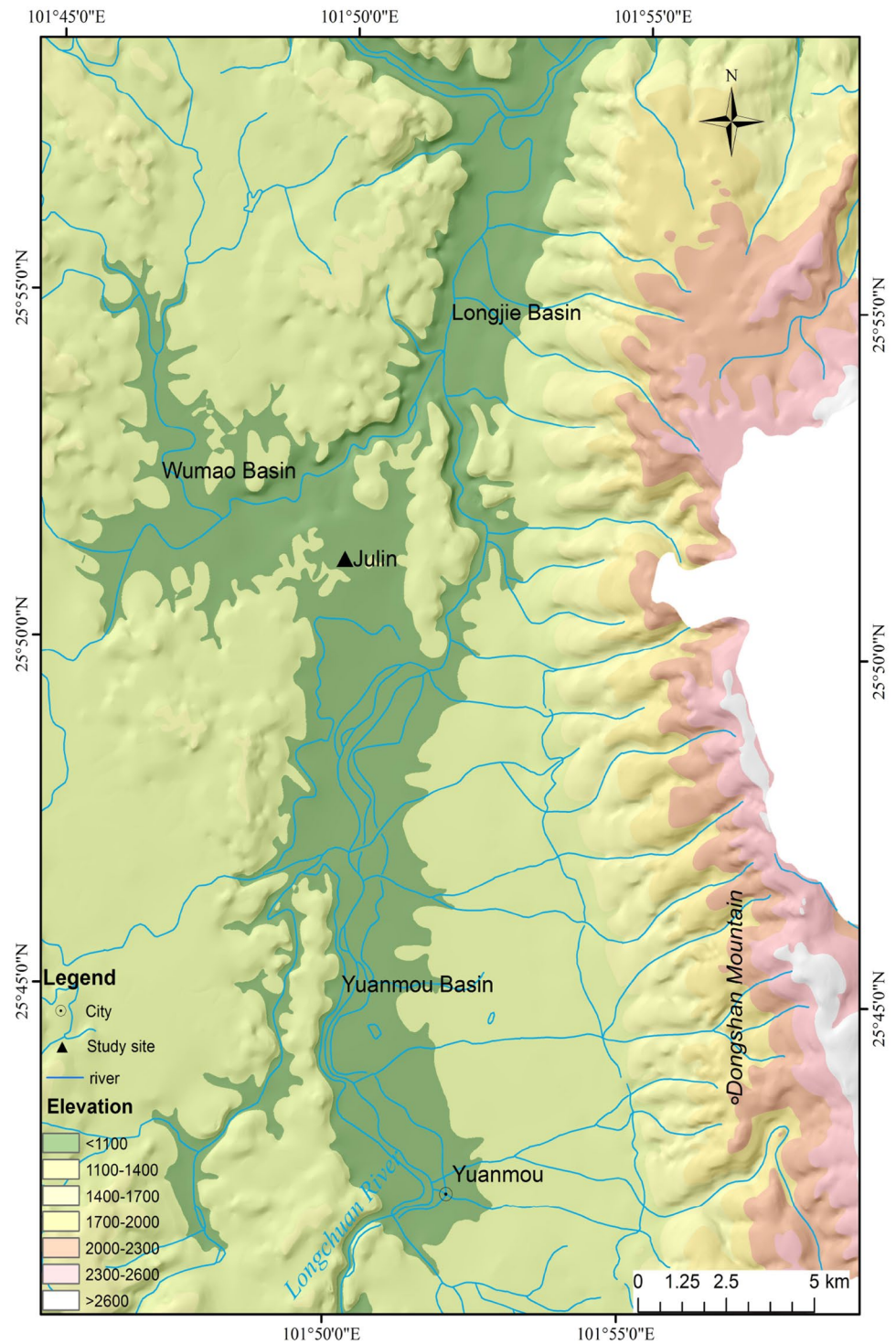
with an average slope gradient of approximately 8°. A supply flume was placed at the top of the plot and a T-shaped collection tank on the bottom; a vertical draining channel was arranged between the flume and tank, with a collecting pool built behind the channel.

Data acquisition

High-flow scouring experiments were conducted in August 2015 at the experimental plot. According to the actual situation of the slope and the rainfall intensity in this area, a
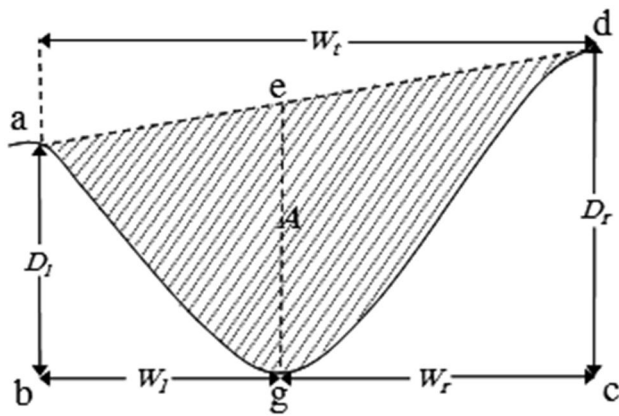
Fig. 2 RCS dimensions

constant discharge flow was set at 10.4 m³/h, the scouring experiments were conducted nine times, and the scouring duration was 25 min. The soil was the typical dry-red soil of the plot, retaining the natural material composition without gravel removal. Soil samples from the plot were used to measure soil particle size. Data from 15 air-dried sieved soil samples demonstrated that the soil particle size distribution in the plot was mainly characterized by aggregates and soil blocks, with four particle sizes (0.2–0.5, 0.5–1, 1–2, and 2–4 cm) accounting for 21.94%, 16.84%, 24.5%, and 27.53%, respectively. According to measurements collected with a JL-1177 laser particle size analyzer, soil clay content was 27.88%, silt content was 51.7%, sand grain content was 20.42%, and the longest axis of the soil gravel in the plot reached 10 cm. Prior to the scouring experiments, the vegetation in the plot was cleared, and the site was preliminarily leveled and artificially trampled. A 10-day waiting period was implemented prior to experiments to allow the surface to reach that of a real slope. Subsequently, the original terrain of the unvegetated plot was scanned with a 3D laser scanner. Characteristic points were set at 0.5, 1, 2, 3, 5, 7, 9, 11, 13, 15, 17, and 19 m away from the rill head to position the RCS. Flow measurements were performed with an LZ-80B glass rotameter during the scouring experiments. Water flowed into the supply flume through the diversion pipe and then into the plot through a 10-cm-wide opening cut out at the supply flume. Rill width, rill depth, runoff width, runoff depth, flow rate, and water temperature at each cross-section were measured and recorded continuously until the termination of water discharge. After the end of each scouring experiment, the surface topography of the plot was scanned with a 3D laser scanner to obtain point cloud data (Fig. 3).

Data processing

Point cloud data were imported into RiSCAN_PRO software and sequentially subjected to splicing–accuracy correction–denoising–vegetation filtering–point cloud vectorization to obtain the complete point cloud data of the plot slope in the same coordinate system in which invalid points were eliminated. The processed point cloud data were imported into ArcGIS 10.2 software and processed through the "Export elevation point data–Create TIN–TIN to Raster" procedures to generate a high-precision DEM of the slope surface. The bottom line of the rill was extracted using the hydrology toolset. Using the 3D Analyst's profile function, a 3D line perpendicular to the water flow direction was generated at each cross-section, and subsequently, a cross-sectional view of the profile was generated. The cross-section coordinates were exported into Excel; various RCS morphologies of the rill were extracted and their correlations were analyzed using linear fitting. Finally, the cross-sectional morphological parameters were calculated in South CASS software. In this study, ten parameters (D_l, D_r, W_t, W_l, W_r, $R_{w/d}$, A, A_w, S_f, and η) were selected to analyze the temporal–spatial variation characteristics of RCS erosion patterns.

Fig. 3 Pictures of the field scouring experiment

Fig. 4 Temporal variations in RCS morphology
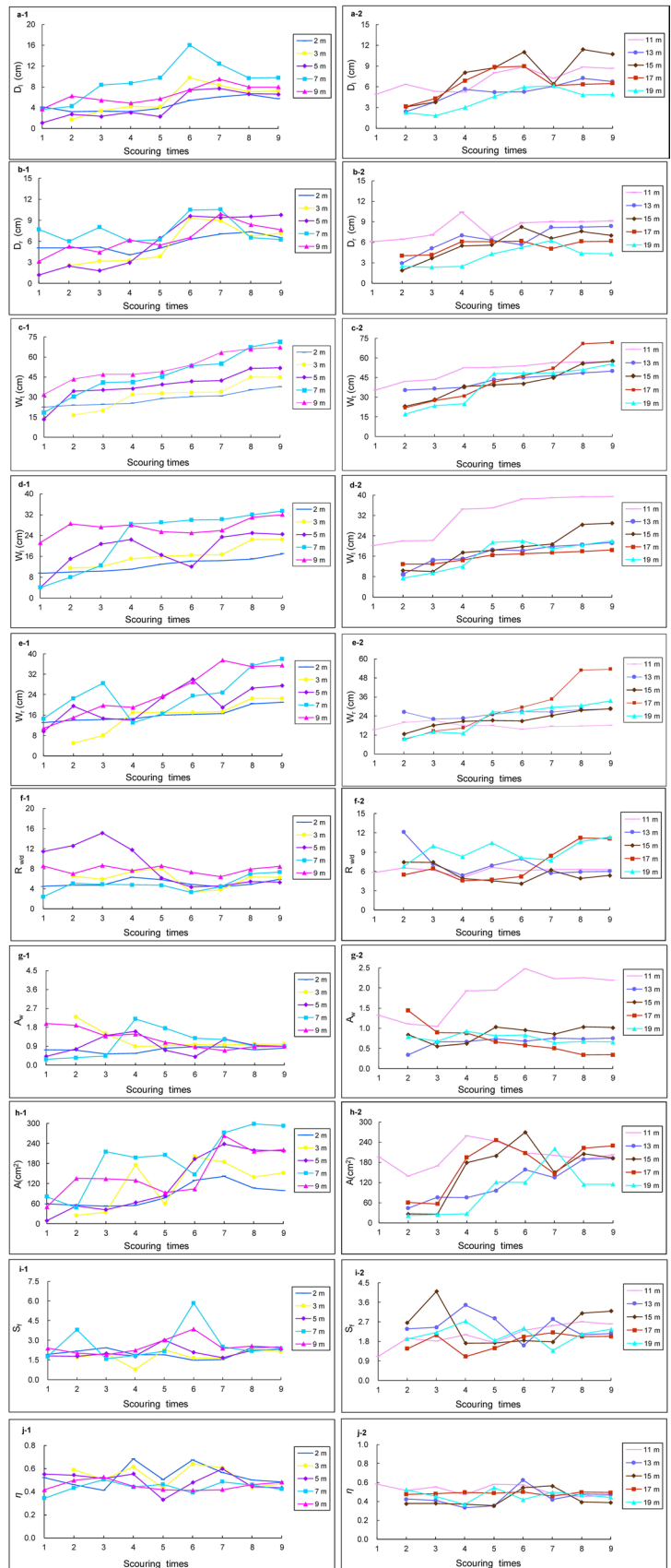
Temporal variation in RCS

Rill depth (D)

Depth of the left side (D_l)

In general, the D_l of the RCS tended to increase significantly with increasing scouring times (Fig. 4). The magnitude of the left depth of various sections varied considerably during rill formation. Excluding cross-sections at 2 and 11 m, the increase in D_l for the remaining cross-sections gradually decreased over time, and the deep-cutting erosion at the left side of the rill gradually weakened. Throughout the experiments, the minimum value of D_l ranged between 1.1 and 4.9 cm for the ten monitored cross-sections, while the maximum was between 6.1 and 11.6 cm. Sediment accumulation appeared at the cross-section at 5 m after experiment 1, with the D_l of the section reaching the minimum. For the cross-section at 7 m, deep-cutting erosion intensified gradually after experiment 6, showing a maximum value of the D_l. No obvious channel formation was observed at the cross-sections at 3, 13, 15, 17, and 19 m after experiment 1, which was still in the slope erosion stage. In contrast, the cross-sections at 2, 7, 9, and 11 m formed apparent channels after experiment 1. Only the cross-section at 13 m reached the maximum left depth of 6.8 cm after the last experiment, while the maximum values for the remaining cross-sections all appeared during the scouring process. After rill formation, the largest was the cross-section at 15 m, with a left depth of 10.7 cm, and the smallest was measured at 19 m, with a left depth of only 4.9 cm.

Depth of the right side (D_r)

Consistent with D_l, the D_r of the RCS generally increased with longer scouring times (Fig. 4). The increase in the D_r decelerated gradually over time for all cross-sections, apart for those at 2, 5, and 7 m. During scouring, the minimum right depth of the cross-sections was between 1.2 and 6.1 cm, whereas the maximum values ranged between 5.6 and 10.5 cm. Similar to the change in D_l, the minimum value of D_r occurred after experiment 1 at the 5-m cross-section. After experiment 7 at the 7-m cross-section, the deep-cutting erosion of the rill intensified, and D_r reached a maximum. After rill formation, the largest was the cross-section at 5 m, with a right depth of 9.8 cm. The cross-section at 19 m exhibited a right depth of merely 4.3 cm due to reduced runoff erosion intensity and sediment accumulation in the upper stream.

Rill width (W)

Top width (W_t)

As shown in Fig. 4, the W_t significantly increased over time and varied between 45 and 71.9 cm during scouring. For the cross-section at 11 m, the W_t formed after each scouring experiment differed only slightly, with no significant changes in size or morphology. The increase in the top width of cross-sections gradually decelerated over time, apart from those at 7, 11, 13, and 17 m. Among the formed rills, the top widths of the cross-sections at 7 and 17 m reached 71.3 and 71.9 cm, respectively, with the variations presenting a slowly increasing trend with longer scouring times. After forming cross-sections, the rills developed gradually toward the shallow trench stage with intensifying lateral erosion. Among the completely formed RCS, excluding those at 7 and 17 m, the cross-section at 2 m was the smallest with a W_t of 37.9 cm and the cross-section at 9 m was the largest with a top width of 67.4 cm.

Left width (W_l)

The W_l tended to increase over time (Fig. 4). The increase in the W_l for cross-sections at 2, 3, 9, 15, and 19 m gradually accelerated over time. Only the cross-section at 5 m exhibited a gradual decelerating increase in W_l over time, while the remaining sections maintained the same growth rate. At the conclusion of the experiment, the minimum W_l was found at the cross-section at 2 m with a value of 17 cm; the maximum W_l was found at 11 m with a value of 39.5 cm. These results indicate that the cross-section at 11 m had the strongest leftward erosion, while that at 2 m was in the initial stage of rill development, showing the weakest leftward erosion.

Right width (W_r)

Similar to the variation trends in W_l, the W_r increased with longer scouring times (Fig. 4). Throughout the experiment, the W_r growth rate remained unchanged for the cross-sections at 2 and 13 m, increased gradually for the cross-section at 17 m, and decreased gradually for the remaining sections, thus eventually forming RCS with relatively stable sizes. The profiles at 5, 7, and 11 m maintained a decreasing trend during the entire scouring test cycle, which is mainly attributed to subjective factors such as an artificially determined rill shoulder line in the scouring process. The minimum W_r was found at the cross-section at 11 m with a value of 17.9 cm, while the maximum W_r was found at 17 m with a value of 53.5 cm. This contrast indicates that rightward erosion was strongest at the cross-section at 17 m and weakest at 11 m. During rill development, W_r (17.9–53.5 cm) varied more

widely than W_l (17–39.5 cm), suggesting greater changes in the W_r of the RCS during the scouring process and more severe rill erosion.

Rill width/depth ratio ($R_{w/d}$)

During the scouring experiments, $R_{w/d}$ values at the various cross-sections were mainly in the 2.41–15.15 range, with a mean of 6.73; therefore, all were characterized as wide-shallow shaped. Among them, the $R_{w/d}$ of cross-sections at 5, 13, and 15 m tended to decrease with longer scouring times at a gradually decelerating pace. This trend indicates that in the early stage of rill development, the channels were dominated by lateral erosion and supplemented by deep-cutting erosion, where the rate of increase in the top width was considerably greater than that for depth. After a certain extent of channel widening, deep-cutting erosion prevailed instead, supplemented by lateral erosion. The cross-sectional depth grew gradually at a rate faster than the top width. The $R_{w/d}$ values of cross-sections at 7, 17, and 19 m grew with longer scouring times, and the rate of growth also gradually slowed and tended to stabilize. At the early stage of the scouring experiment, the channels at the corresponding sections produced branch channels, and with the continuous development of rills, the branch channels merged to widen the profiles, resulting in a gradual increase in the $R_{w/d}$ of the profiles. The $R_{w/d}$ values of the remaining characteristic cross-sections differed only slightly throughout the experiment, indicating that the cross-sectional width and depth of rills grew at a substantially uniform rate during rill development and their sizes increased gradually, while morphological differences were small.

Width asymmetry ratio (A_w)

Overall, A_w values initially decreased and then increased over time. The left and right erosion directions fluctuated, and the RCS had a strong asymmetry. The A_w values for cross-sections at 2, 11, 13, and 15 m generally increased with longer scouring times, while the remaining cross-sections showed a decreasing trend. Therefore, leftward erosion was faster than the rightward erosion at 2, 11, 13 and 15 m, and vice versa for the remaining RCS. From a statistical perspective, A_w values for various cross-sections ranged between 0.28 and 2.48 during the experiment, and the directions of leftward and rightward erosions were rather complicated. Overall, left side erosion prevailed at 7, 9, 11, and 15 m, while the remaining six sections were dominated by right side erosion. At the conclusion of the experiment, left-leaning cross-sections formed at 11 and 15 m, while the remaining developed into right-leaning cross-sections.

Cross-sectional erosional area (A)

The erosional area of the RCS significantly changed with scouring times (Fig. 4). Specifically, all cross-sections, excluding that at 11 m, showed a highly significant increase with longer scouring times. The erosion size of the rill increased, and the erosion degree also continued to intensify. The increase in erosional area accelerated gradually over time for cross-sections at 3, 5, 15, and 19 m, decelerated gradually for those at 9, 13, and 17 m, and remained stable for those at 2 and 7 m. During the experiment, the minimum erosional area of the ten characteristic cross-sections ranged between 8.8 and 139.3 cm^2, whereas the maximum areas were 141.2–298.2 cm^2. The difference between the maximum and minimum values of RCS was smallest at 2 m, accounted for 76.9 cm^2, followed by 11 m, with a value of 120.1 cm^2, and the largest at 7 m, accounted for 250.4 cm^2. These results indicate that the cross-sections at 2 and 11 m had the least changes in shape and size during the scouring, while that at 7 m was subject to the greatest changes. Among the stable channels formed at the conclusion of the experiment, the smallest erosional area was found at the cross-section at 2 m, 98.6 cm^2, while the largest was found at 7 m, 292.7 cm^2. Therefore, the cross-section at 2 m was the smallest in size and had the lowest erosion degree, while that at 7 m was the largest in size, with the highest erosion degree.

Rill shape

Shape factor (S_f)

S_f values of the RCS ranged between 0.78 and 3.95, and the shapes were mainly parabolic, triangular, and intermediate from parabolic to triangular. In the initial stage of the scouring experiment, the cross-sectional shapes at 2, 3, 5, 11, and 19 m were intermediate from parabolic to triangular. Cross-section shapes at 2, 3, 5, and 11 m showed complexity and uncertainty, with various shapes appearing over time. All remaining cross-sections were primarily triangular-shaped throughout rill development, while the intermediate shape from parabolic to triangular appeared less than twice. At the end of the experiment, S_f values for all cross-sections were greater than 2.0, and their shapes were all triangular.

Shape ratio (η)

The shape ratios increased or decreased with longer scouring times, with a slight upward trend at 2, 7, 13, 15, and 17 m, and a slight downward trend for the remaining profiles. The RCS morphology types included wide-shallow, narrow-deep, intermediate, and isosceles triangle shapes. In the early stage of rill development, η values for cross-sections at 3, 5, 11, and 19 m were between 0.52 and 0.59, and the final η values ranged

from 0.43 to 0.47. Therefore, during the scouring experiment, their cross-sectional shapes transitioned from wide-shallow shaped to isosceles triangle and then to narrow-deep shaped. For the cross-section at 9 m, η values were all between 0.41 and 0.53, with no significant changes in morphology. After the experiment, η values for cross-sections at 2 and 9 m were both 0.48, and their shapes approximated isosceles triangles.

RCS spatial variation along the rill

Rill depth (D)

Left depth (D_l)

After the first experiment, only five characteristic cross-sections, at 2, 5, 7, 9, and 11 m, on the slope formed small drop pits or intermittent wide-shallow grooves. The changes in D_l values along the course for various sections tended to increase first and then decreased after experiments 2, 3, and 7. In 4–6 and 8–9 experiments, D_l values for various sections presented an alternating increase–decrease–increase pattern and generally reached local maxima at interval sections, i.e., 3, 7, 11, and 15 m. Overall, the local extrema of the RCS fluctuated slightly, and the position of the maximum D_l value was closer to the rill head. Due to various environmental factors and different hydrodynamic conditions, the cross-sections showed varying erosion rates at different rill segments, i.e., upper, middle, and lower, and the erosion degrees also varied.

Right depth (D_r)

Similar to the variation in D_l, after experiments 2–4 and 7, D_r values for various cross-sections from rill head to mouth showed an increase-then-decrease trend, reaching maxima at 7 and 5 m. After experiment 5, small value ranges were observed in D_r for various cross-sections. In experiment 6, in contrast, the D_r exhibited an alternating increase–decrease–increase pattern, and the maximum value remained at the cross-section at 5 m. In the later stage of the experiment, variations in D_r presented an alternating increase–decrease–increase–decrease pattern. In addition, two crests appeared in the middle of the rill, and the crest values were located at cross-sections at 5 and 9 m, reaching the maximum at 9 m (Fig. 5).

Rill width (W)

Top width (W_t)

W_t values showed significant differences during each experiment and a unique variation along the course (Fig. 5). After experiments 2–4, cross-sections on the slope showed

three crests and three troughs, with maxima at 5, 11, and 17 m. After experiments 6–9, the cross-sections presented two crests and two troughs and wide-shallow alternating trends along the rill from head to mouth. The maxima appeared at cross-sections at 7, 9, and 17 m, while local maxima and minima appeared in the crest and trough positions, respectively. W_t values for various cross-sections changed only slightly along course during experiment 5. The cross-sections roughly presented an N-pattern along the course, i.e., increase–decrease–increase during experiments 5–7, but exhibited an M-pattern, i.e., increase–decrease–increase–decrease during experiments 8–9.

Left width (W_l)

Figure 5 indicates that the W_l values of various RCS varied substantially during the scouring process. After experiments 2–3 and 7–9, W_l values generally showed an increase–decrease–increase–decrease trend along course and reached local maxima and minima at different profiles; of these, the local maxima were distributed roughly in the middle and lower rill segments (7–15 m). During experiments 4–5, the W_l values of various cross-sections exhibited an alternating narrow–broad–narrow pattern along course, all of which reached local maxima at 11 and 15 m. W_l values for various cross-sections fluctuated less intensely along the course of the experiment than in the initial experimental stage, with relatively stable changes.

Right width (W_r)

W_r values for various cross-sections changed less considerably along course than W_l (Fig. 5). Overall, in the early stage of rill development (experiments 2–7), W_r values of the profiles were lower than in later experiments, e.g., 8–9, and the difference values between adjacent profiles were fairly small. Moreover, a waxing and waning feature was present within a relatively short distance. In the later stages of rill development, variations in W_r values along course were represented by the three crests and three troughs, and local maxima appeared at 9, 13, and 17 m. The values of cross-sections at various rill locations tended to broaden in a spiral shape along course from rill head to mouth.

Rill width/depth ratio ($R_{w/d}$)

As shown in Fig. 5, $R_{w/d}$ values fluctuated along the course of the experiment. In the early stage of rill development, $R_{w/d}$ values for various cross-sections changed significantly, tending to decrease from rill head to mouth. Changes in the ratio were quite small in the later stage of rill development, with a tendency to increase gradually from rill head
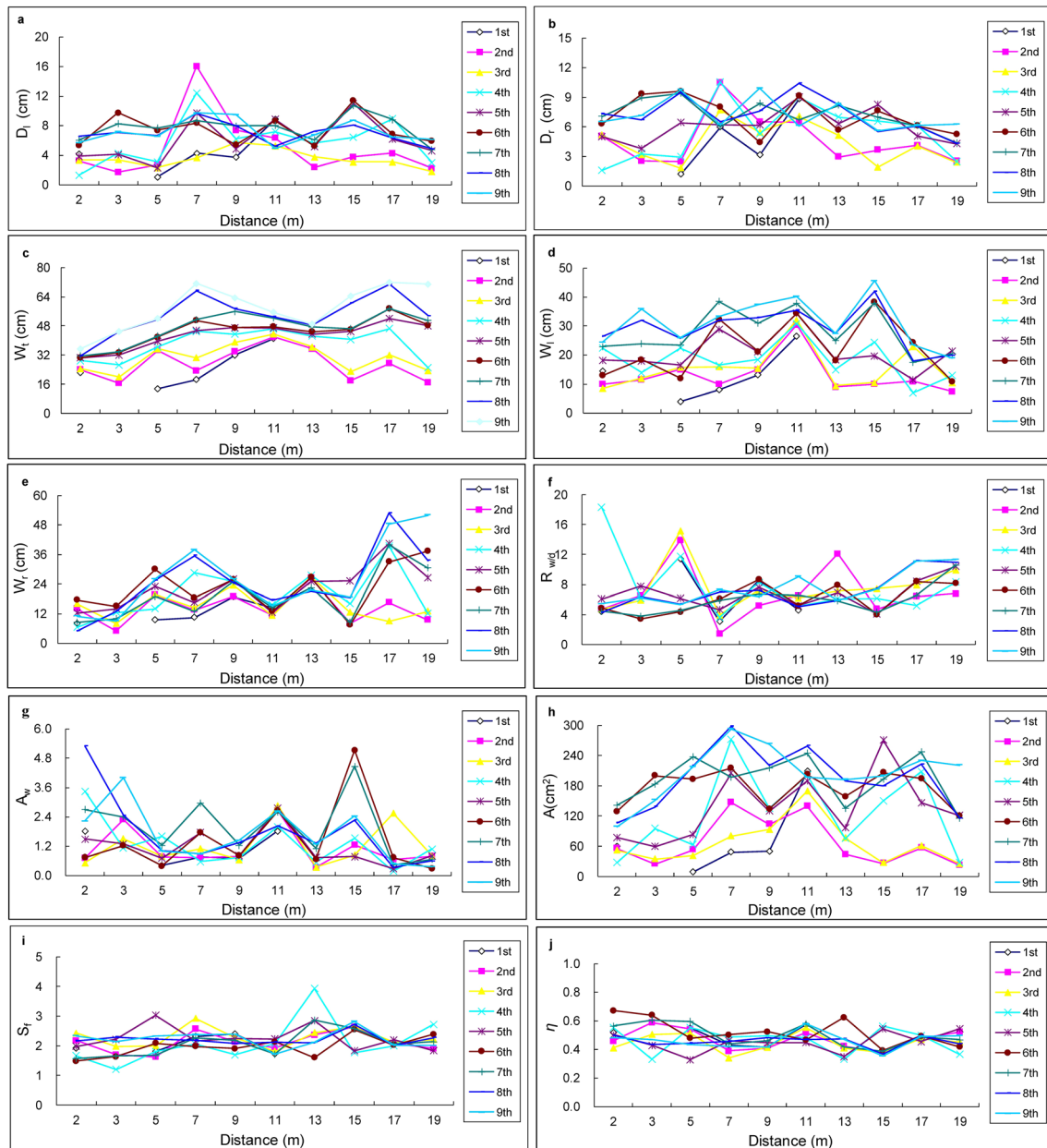
Fig. 5 Spatial variations in RCS morphology

to mouth. After experiment 2, $R_{w/d}$ values reached local maxima at 5 and 13 m. After experiment 3, $R_{w/d}$ values showed a gradually decreasing trend for 5 m cross-section, while increasing gradually at the 7 m cross-section. After experiment 6, $R_{w/d}$ values for the cross-sections at 3, 5, and 15 m reached minima, while during experiments 7–9, values again increased continuously. An overall alternating increase–decrease–increase distribution of $R_{w/d}$ values for various profiles indicate that in the early stage of rill development, various cross-sections were dominated by lateral erosion and supplemented by deep-cutting erosion. Moreover, the rate of lateral erosion was faster than that of

deep-cutting erosion, resulting in greater $R_{w/d}$ values for the cross-sections. After the lateral erosion reached a certain level, the primary rill erosion mode shifted to deep-cutting erosion, with supplementary lateral erosion, i.e., the rate of deep-cutting erosion was faster than that of lateral erosion. After rill development concluded, all cross-sections were dominated by lateral erosion.

Width asymmetry ratio (A_w)

A_w values were highly asymmetric, and the direction and degree of erosion changed frequently (Fig. 5). After

experiments 2–5, cross-sections exhibited larger A_w values, and the number of positions where the local maxima occurred along the course initially increased and then decreased. In addition, the ratio values also decreased gradually and then tended to stabilize, indicating a more severe degree of rill right side erosion. After experiment 6, the A_w for cross-sections near the rill head changed smoothly along course, with local maxima only at 7 m, while the remaining ratios were minimal throughout all scouring experiments. This indicates that the A_w values of various RCS along the course increased as the scouring experiments progressed. As the rill developed, cross-sections at 3, 11, and 19 m developed into left-leaning cross-sections, while the remaining developed into right-leaning cross-sections. Various RCS demonstrated highly asymmetric development along the course.

Cross-sectional erosional area (*A*)

Figure 5 shows that the size and shape of various profiles were highly variable during rill development, with severe erosion. In the initial experiment stage, the *A* values in the upper and lower parts of the rill were lower than those in the middle. After experiments 4–6, difference values for adjacent cross-sectional areas along the course varied significantly, and the shape and size fluctuated drastically. With further rill development, the *A* values for various cross-sections presented a general alternating increase–decrease during experiments 7–9, the size differences reduced, and all values reached maxima at the 7-m cross-section. In short, the erosion sizes for various cross-sections were greater during the later stages of rill development than in the early stages, with generally stable change rates.

Rill shape

Shape factor (S_f)

S_f values either increased or decreased along the slope surface, and the positions of local maxima and minima were unfixed, generally differing by 4 m. In the initial experiment stages, S_f values of various cross-sections varied greatly along course; the large fluctuations, ranging from 1.4 to 3.5, indicate a large difference in shape. Cross-sections varied in size and shape, which manifested as parabolic, intermediate from parabola to triangle, triangular, and narrow-deep shapes. After experiment 8, the rill was basically formed, and the cross-sectional morphology stabilized, with the form of a gentle curve along course. Eventually, all cross-sections reached an S_f value of 2.0 and were in fixed shapes (Fig. 5).

Shape ratio (*η*)

In general, *η* values for adjacent RCS differed greatly in the initial stage of the experiment, showing an alternating distribution of three local maxima and two local minima along the course of the experiment (Fig. 5). Among them, local maxima were located at 3, 11, and 19 m. The largest difference in *η* values for adjacent cross-sections was found after experiment 6, where the morphological difference was also greatest. As the experiments progressed, differences in *η* values for adjacent cross-sections decreased gradually and had the lowest values at the end of the experiment. The values the cross-sections along the course presented a gentle curve, and the morphology of various cross-sections showed a wide-shallow shape.

Discussion

This study focused on the cross-section morphology of rills formed in soil interbedded with clay and gravel to analyze the spatio-temporal morphological variations in a Dry-Hot Valley and compare the characteristics. The results generally agree with laboratory experiments, although there are some notable differences due to different test conditions and the unique soil conditions of the Dry-Hot Valley.

Soil texture heterogeneity creates fluctuations in RCS along the rill

Local environment has an influence on rill formation and development, and further restricts the variation in RCS, clarifying regional differences in morphological variations. Studies have demonstrated that soil texture is a key factor on the distribution of RCS along the rill (Sheng et al. 2017; Xue et al. 2016). The soil in the Yuanmou Dry-Hot Valley is a typical dry-red soil with interbedded clay and gravel. Soil aggregates, clods, and gravels with large spatial differences in soil particle sizes; most clods were 2–4 cm and gravels were 8–11 cm in length. Soil compactness varies with a quadratic polynomial with soil depth, but the significance test of the variation is different, and the soil profile is inhomogeneous. Therefore, unique soil materials in the study area create large variations in the morphological parameters of the ten cross-sections along the rill. From Fig. 5, *A* increased sharply at the initial stage of rill depth development, forming an M-shaped distribution along the rill, and the RCS showed alternating left and right side erosion in space. The width of the left and right sides of the rill fluctuated to form M and W shapes, respectively, and the degree of lateral erosion was different. The indices describing RCS, *η*, S_f, and A_w, showed general instability during temporal–spatial variations in scouring. This result is in contrast with

scouring tests in the laboratory on the Loess Plateau, where the morphology of rill cross-sections varied monotonously along the rill (Ma et al. 2017a).

Disequilibrium in rill morphology development under high-flow scouring

Hydrodynamic conditions with highly spatiotemporal variations had some impact on the development and evolution of RCS by interfering with the denudation of rill flow. Based on the high-flow scouring test conditions, the average flow velocity at each RCS was 0.74 m/s, with a decreasing trend at later stages of scouring. The form of runoff varied gradually from turbulent to transition flow with rill development. The RCS morphology rapidly developed in early rill development and then slowed. The same results were obtained during tests on the Loess Plateau (Li et al. 2008; Wang et al. 2014). The experiments also indicated that rill shape indices decreased with increases in hydrodynamic parameters during spatio-temporal variations. This observation disagrees with those from indoor rainfall or scouring experiments on red soil, where variations in rill shape indices showed few trends (Hao et al. 2018). The development and evolution of RCS in real field conditions were nonlinear. In addition, the collapse of the rill bank is attributed to dredging and erosion due to the lack of overland flow effect in the high-flow scouring conditions. Thus, variations in RCS morphology under different dynamic conditions is an important future research direction for the Yuanmou Dry-Hot Valley.

Asymmetry in the variation of cross-sections at different stages of rill development

From the perspective of temporal evolution, increasing scouring duration resulted in highly significant asymmetry in RCS due to differences between left and right erosion directions during development. This result is also in contrast to those from indoor scouring tests on the Loess Plateau, where the shape of the RCS was wide and shallow at the beginning of rill development, followed by narrow and deep (Ma et al. 2017a). Spatially, the instability in erosion direction resulted in RCS morphology with both right-leaning and left-leaning distributions when the rill body and mouth were measured with reference to the width asymmetry ratio. Based on the shape factor ratio, the RCS has an asymmetric sawtooth shape, from parabolic to triangular during rill development. These results were clearly different from those obtained in the field investigation in gully and hilly region of Loess Plateau, where the RCS morphology of rills showed quasi-symmetrical V and U type shapes to small upper opening and large bottom type along with rill development (Wang et al. 1988). There were extreme variations in rill erosion direction and erosional degree for different rill parts, i.e.,

rill head, body, and mouth, and few quasi-symmetrical distributions of cross-sections in the Yuanmou Dry-Hot valley. However, it is not possible to thoroughly measure the degree of asymmetry of RCS using existing morphological parameters, and follow-up studies should focus on systematic indices that characterize the asymmetrical features of cross-sectional morphology.

Conclusions

RCS morphological development in the Yuanmou Dry-Hot Valley, inter-bedded clay and gravel soils, showed clear spatio-temporal differences based on morphological parameters. Under high-flow scouring conditions, spatial variations in RCS morphology were more significant than those of temporal variations. Comparing temporal and spatial evolution of the same parameter, temporal variations in RCS morphology were opposite to spatial variations. In summary, the derived proportional parameters of RCS showed a more complicated development process than size parameters during spatio-temporal variations. Nonlinear fluctuation trends were observed in the variation of RCS on slopes with soils and gravels with significant asymmetry in the shape.

Compliance with ethical standards

Conflict of interest The authors declare that they have no conflict of interest.

References

Bennett SJ (1999) Effect of slope on the growth and migration of headcuts in rills. Geomorphology 30:273–290

Bennett SJ, Gordon LM, Neroni V, Wells RR (2015) Emergence, persistence, and organization of rill networks on a soil-mantled experimental landscape. Nat Hazards 79:7–24

Berger C, Schulze M, Riekezapp D, Schlunegger F (2010) Rill development and soil erosion: a laboratory study of slope and rainfall intensity. Earth Surf Process Landf 35:1456–1467

Bewket W, Sterk G (2003) Assessment of soil erosion in cultivated fields using a survey methodology for rills in the Chemoga watershed, Ethiopia. Agric Ecosyst Environ 97:81–93

Bruno C, Stefano CD, Ferro V (2010) Field investigation on rilling in the experimental Sparacia area, South Italy. Earth Surf Process Landf 33:263–279

Brunton DA, Bryan RB (2015) Rill network development and sediment budgets. Earth Surf Process Landf 25:783–800

Bryan RB, Govers G, Poesenb SRA (1989) The concept of soil erodibility and some problems of assessment and application. CATENA 16:393–412

Cao L, Zhang K, Yin L (2014) Factors affecting rill erosion of unpaved loess roads in China. Earth Surf Process Landf 39:1812–1821

Capra A, Stefano CD, Ferro V, Scicolone B (2010) Similarity between morphological characteristics of rills and ephemeral gullies in Sicily, Italy. Hydrol Process 23:3334–3341

Eltner A, Baumgart P, Maas HG, Faust D (2015) Multi-temporal UAV data for automatic measurement of rill and interrill erosion on loess soil. Earth Surf Process Landf 40:741–755

Foster GR (1982) Modelling the erosion process. In: Haan CT, Johnson HP, Brakensiek DL (eds) Hydrologic modeling of small watersheds, ASAE Monograph No. 5, American Society of Agricultural Engineers, St. Joseph, pp 297–380

Frankl A, Poesen J, Scholiers N, Jacob M, Haile M, Deckers J, Nyssen J (2013) Factors controlling the morphology and volume (*V*)—length (*L*) relations of permanent gullies in the Northern Ethiopian Highlands. Earth Surf Process Landf 38:1672–1684

Gabet EJ, Bookter A (2008) A morphometric analysis of gullies scoured by post-fire progressively bulked debris flows in southwest Montana, USA. Geomorphology 96:298–309

Gao P (2011) Mountain and hillslope geomorphology|Hillslope erosion: rill and gully development processes. In: Shroder J (ed) Treatise on geomorphology. Elsevier, San Diego

Gilley JE, Kottwitz ER, Simanton JR (1990) Hydraulic characteristics of rills. Trans Asae 33:1900–1906

Giménez R, Planchon O, Silvera N, Govers G (2010) Longitudinal velocity patterns and bed morphology interaction in a rill. Earth Surf Process Landf 29:105–114

Govers G (1992) Relationship between discharge, velocity and flow area for rills eroding loose, non-layered materials. Earth Surf Process Landf 17:515–528

Green AN, Goff JA, Uken R (2007) Geomorphological evidence for upslope canyon-forming processes on the northern KwaZulu-Natal shelf, SW Indian Ocean, South Africa. Geo Mar Lett 27:399–409

Hao H, Guo Z, Wang X, Zhan H, Ma R, Li Z, Jiang J (2017) Rill erosion process on red soil slope under interaction of rainfall and scouring flow. Trans Chin Soc Agric Eng 33:134–140

Hao H, Guo Z, Li Z, Hua L (2018) Characteristics of rill cross-section morphology and hydrodynamics on red soil slope. Res Environ Yangtze Basin 27:363–370

He J-J, Ye LU, Li GH, Cai QG (2013) Experimental study on rill erosion characteristics and its runoff and sediment yield process. J Hydraul Eng 44:398–405

He J-J, Sun LY, Gong HL, Cai QG, Jia LJ (2016) The characteristics of rill development and their effects on runoff and sediment yield under different slope gradients. J Mt Sci 13:397–404

Heede B (1970) Morphology of gullies in the Colorado rocky mountains. Int Assoc Sci Hydrol Bull 15:79–89

Li H (2015) Study on the evolution of rill cross section morphology. Northwest Sci Tech Univ Agric For. Thesis for Master's Degree, Xi'an City, China

Li Z, Qing B, Kang W, Li P, Li W, Wei X (2008) Indoor experimental studies on hydrodynamic characteristics of runoff in rill erosion procession steep slope. Trans Chin Soc Agric Eng 24:64–68

Liu Y, Zhu X, Zhou P, Tang K (1988) The laws of hillslope channel erosion occurrence and development on Loess Plateau. Res Soil Water Conserv 7:9–18

Loch RJ, Donnollan TE (1989) Rill erosion of a self-mulching black earth.1. Effects of tillage Australian. J Soil Res 27:525–534

Ma X, Zhang K, Yang F, Yang M, Dong X (2017a) Influencing factor analysis of rill erosion section morphology development on slope and its dynamic characteristic experiment. Trans Chin Soc Agric Eng 33:209–216

Ma X, Zhang K, Yang F, Yang M, Dong X (2017b) Influencing factor analysis of rill erosion section morphology development on slope and its dynamic characteristic experiment. Trans Chin Soc Agric Eng 33(208):209–216

Mahmoodabadi M, Ghadiri H, Yu B, Rose C (2014) Morpho-dynamic quantification of flow-driven rill erosion parameters based on physical principles. J Hydrol 514:328–336

Mancilla GA, Chen S, Mccool DK (2005) Rill density prediction and flow velocity distributions on agricultural areas in the Pacific Northwest. Soil Tillage Res 84:54–66

Meyer LD, Foster GR, Huggins LF (1984) A laboratory study of rill hydraulics: 1. Velocity relationships. Trans Asabe 27:790–796

Moore ID, Burch GJ (1986) Sediment transport capacity of sheet and rill flow: application of unit stream power theory. Water Resour Res 22:1350–1360

Nearing MA, Foster GR, Lane LJ, Finkner SC (1989) A process-based soil erosion model for USDA-Water Erosion Prediction Project technology. Trans Asae 32:1587–1593

Ran H, Deng Q, Zhang B, Hui L, Lei W, Luo M, Qin F (2018) Morphology and influencing factors of rills in the steep slope in Yuanmou Dry-Hot Valley (SW China). CATENA 165:54–62

Rejman J, Brodowski R (2010) Rill characteristics and sediment transport as a function of slope length during a storm event on loess soil. Earth Surf Process Landf 30:231–239

Rustomji P (2006) Analysis of gully dimensions and sediment texture from southeast Australia for catchment sediment budgeting. CATENA 67:119–127

Shen H, Zheng F, Wen L, Jia L, Jiang Y (2015a) An experimental study of rill erosion and morphology. Geomorphology 231:193–201

Shen H, Zheng F, Wen L, Jiang Y, Jia L (2015b) Effects of rainfall intensity and slope gradient on rill morphological characteristics. Trans Chin Soc Agric Mach 46:162–170

Sheng H, Sun L, Cai Q (2017) Impact of rill morphology on hillslope erosion for Loess soils. J Basic Sci Eng 25:679–688

Slattery MC, Bryan RB (1992) Laboratory experiments on surface seal development and its effect on interrill erosion processes. Eur J Soil Sci 43:517–529

Stefano CD, Ferro V, Pampalone V, Sanzone F (2013) Field investigation of rill and ephemeral gully erosion in the Sparacia experimental area, South Italy. CATENA 101:226–234

Stefano CD, Ferro V, Pampalone V (2016) Measuring field rill erodibility by a simplified method. Land Degrad Dev 27:239–247

Stefano CD, Ferro V, Palmeri V, Pampalone V (2018) Testing slope effect on flow resistance equation for mobile bed rills. Hydrol Process 32:664–671

Wang G, Bai Y, Jia Z, Wei Z, Li J (1988) A preliminary study on the characteristics of the development and erosion of the rill. Soil Water Conserv China 5:13–16

Wang L, Cai Q, Cai C, Sun L (2014) Morphological changes of rill on loess slope and its relationship with flow velocity. Trans Chin Soc Agric Eng 30:110–117

Wang J, Li H, Meng Q, Wang Y, Zhang Q (2015) Characteristics of rill cross section morphology, hydrodynamics and sediment-carrying capacity on Loess slopes. J Soil Water Conserv 29:32–37

Xue J, Wang J, He LI, Wang Y, Zhou M (2016) Experimental analysis of development regularities of rill erosion on heavy silty loam sloping surface. J Irrig Drain 35:69–72

Yan D, Wen A, Shi Z, Ming SU, He X (2010) Critical slope length and control of rill occurrence on cultivated land of purple soil in Sichuan Basin. Res Soil Water Conserv 17:1–4

Yang M, Walling DE, Tian J, Liu P (2006) Partitioning the contributions of sheet and rill erosion using beryllium-7 and cesium-137. Soil Soc Am J 70:1579–1590

Yermolaev OP, Gafurov AM, Usmanov BM (2018) Evaluation of erosion intensity and dynamics using terrestrial laser scanning. Eurasian Soil Sci 51:814–826

Yuan L, Chang C (2008) A cellular automata approach to the simulation of rill self-organizing development process on hillslope. Res Soil Water Conserv 15:7–9

Zhang K, Tang K (2000) A study on hydraulic characteristics of flow for prediction of rill detachment capacity on loess slope. Acta Pedol Sin 37:9–15

Zhang Y, Wu Y, Liu B, Zheng Q, Yin J (2007) Characteristics and factors controlling the development of ephemeral gullies in cultivated catchments of black soil region, Northeast China. Soil Tillage Res 96:28–41

Zhang F, Yang M, Walling DE, Zhang B (2014) Using Be-7 measurements to estimate the relative contributions of interrill and rill erosion. Geomorphology 206:392–402

Zhang P, Yao W, Tang H, Xiao P (2018) Rill morphology change and its effect on erosion and sediment yield on loess slope. Trans Chin Soc Agric Eng 34(116):114–119

Publisher's Note Springer Nature remains neutral with regard to jurisdictional claims in published maps and institutional affiliations.